# Late time sharp transitions in an embedded universe

**Abraao J.S Capistrano**

1. Federal University of Latin-American Integration, 85867-970, Foz do Iguaçu-PR, Brazil

E-mail: abraao.capistrano@unila.edu.br

September 2019

**Abstract.** Using a joint statistical analysis, we test a four-dimensional FLWR model embedded in a five-dimensional bulk based on the Nash-Greene embedding theorem. Performing a Markov Chain Monte Carlo (MCMC) modelling, we combine observational data sets as those of the recent Pantheon type Ia supernovae, Baryon Acoustic Oscillations (BAO) and the angular acoustic scale of the Cosmic Microwave Background (CMB) to impose restrictions on the model and correlating the model parameters to mimick an equation of state. From statistical classifiers as the Akaike Information Criterion (AIC) and Bayesian Information Criterion (BIC), we use the Jeffreys' scale and find a strong evidence favoring a statistically consistence with a dynamical Dark energy (CPL parameterization) and a relative consistence with both $\Lambda$CDM and $w$CDM models. Moreover, we find that the transition redshift used as a cosmic discriminator with the best fit $z_t = 0.634 \pm 0.014$ at 1-$\sigma$ C.L. with a range scenario for late time sharp transitions.

*Keywords*:modified Friedman equations, modified gravity, dark energy

## 1. Introduction

The true mechanism behind the accelerated phase of the universe remains an open question. After more than 20 years since the very first evidences of the cosmic accelerated expansion, one of the pivotal directions of investigations is about to unravel whether the dark energy equation of state (EoS), with the main fluid parameter $w(z)$, is restricted to the value $w_0 = -1$, as suggested by observations [1], in conformity with the very popular $\Lambda$CDM model, or if there exists any deviations from that value leading to dynamical dark energy models. Even though its success, the $\Lambda$CDM model lacks of an underlying physical understanding, since the Cosmological constant $\Lambda$ and the Cold dark matter (CDM) are problems of their own [2, 3, 4, 5, 6, 7, 8]. Hence, an equation of state plays a fundamental role to confront a model to the observational data commonly performed with statistical methods. Interestingly, it has been suggested that the dark energy equation may have a late-time phase transition [9, 10, 11] with $z \gtrsim 1$. This induces to an interesting scenario departing from the non-dynamical $\Lambda$CDM cosmology since at high redshifts the constraints are weaker [10, 12, 13, 14, 15, 16, 17, 18].

The theoretical background in this paper concerns the possibility that the universe might be embedded in extra dimensions and dark energy can be explained as a geometric outcome from the extrinsic curvature. Most of these extra dimensional models have been Kaluza-Klein or/and string inspired, such as, for instance, the Arkani-Hamed, Dvali and Dimopolous (ADD) model [19], the Randall-sundrum model [20, 21] and the Dvali-Gabadadze-Porrati model (DPG) [22]. Differently form these models and variants, we investigate how the embedding as a prior mathematical structure can be suited for construction of a physical theory, keeping no relation with brane or string proposals. Several authors have been explored this possibility in many contexts [23, 24, 25, 26, 27, 28, 29, 30, 31, 32, 33, 34].

This paper aims at investigating in a late-time transition redshift on how the cosmological parameters, mainly on the current matter density $\Omega_{m0}$ and the physical baryon density $100\Omega_b h^2$, are accommodated in the presented model under this assumption and whether the current surveys on dark energy constrain the parameters to favor or not a phase transition over some popular models as the ΛCDM, quintessense ($w$CDM) [35, 36] and Chevallier-Polarski-Linder (CPL) [37, 38] parameterisations. To analyse the background data, we perform the Markov Chain Monte Carlo (MCMC) sample technique with a modified code from [39, 40] using the joint likelihood of kinematical probes as of the Cosmic Microwave Background (CMB) Planck 2015 data [1], the largest dataset Pantheon SnIa [41] with redshift ranging from $0.01 < z < 2.3$ that guarantees a low and intermediate redshift data, the Hubble parameter as a function of redshift ($H(z)$)[42, 43, 44, 45, 46, 47] and Baryonic Acoustic Oscillations (BAO) from points of the joint surveys 6dFGS [48], SDDS [49], BOSS CMASS [50], WiggleZ [51], MSG [52] and BOSS DR12 [53].

The paper is organized as follows: in the second section, we make a review on the theoretical framework. The third section presents the cosmological analysis and outcomes by using the Akaike Information Criterion [54] and Bayesian criteria [55] on the resulting contours confidence regions. In the final section, we conclude with our final remarks and prospects.

## 2. The theoretical framework

### *2.1. The D-dimensional equations*

We start with a summary of main elements of a gravitational model based on the mathematical background of the theory of dynamical embeddings. The first mechanism is the defined by the gravitational action functional. Thus, in the presence of confined matter fields on a four-dimensional space with thickness $l$ embedded in a D-dimensional ambient space (bulk), we define

$$S = -\frac{1}{2\kappa_D^2}\int\sqrt{|\mathcal{G}|}\mathcal{R}d^Dx - \int\sqrt{|\mathcal{G}|}\mathcal{L}^*_m d^Dx \ , \tag{1}$$

where $\kappa_D^2$ is the fundamental energy scale on the embedded space, $\mathcal{R}$ denotes the Ricci scalar of the bulk and $\mathcal{L}^*_m$ is the confined matter lagrangian. The normal radii $l$ is the smallest value of the curvature radii obtained from the relation

$$det(g_{\mu\nu} - l^a k_{\mu\nu a}) = 0 \ . \tag{2}$$

In a geometrical sense, the term $y^a = l^a$ represents a displacement of the embedded space along the extra-dimensions.

The matter energy momentum tensor occupies a finite hypervolume with constant radius $l$ along the extra-dimensions. The variation of Einstein-Hilbert action in eq.(1) with respect to the bulk metric $\mathcal{G}_{AB}$ leads to the Einstein equations for the bulk

$$\mathcal{R}_{AB} - \frac{1}{2}\mathcal{G}_{AB} = \alpha^\star \mathcal{T}_{AB} \ , \tag{3}$$

where $\alpha^\star = 8\pi G^*$ is energy scale parameter and $G^*$ is the bulk "gravitational constant". The tensor $\mathcal{T}_{AB}$ is the energy-momentum tensor for the bulk [25, 26, 29]. To generate a thick embedded space-time is important to perturb the related background and can be done using the confinement hypothesis that depends only on the four-dimensionality of the space-time [56, 57, 58], even though any gauge theory can be mathematically constructed in a higher dimensional space.

In order to obtain a more general theory based on embeddings to elaborate a physical model, Nash's original embedding theorem [59] used a flat D-dimensional Euclidean space, later generalized to any Riemannian manifold including non-positive signatures by Greene [60] with independent orthogonal perturbations. This choice of perturbations facilitates to get to a differentiable smoothness of the embedding between the manifolds, which is a primary concern of Nash's theorem and satisfies the Einstein-Hilbert principle, where the variation of the Ricci scalar is the minimum as possible. Hence, it guarantees that the embedded geometry remains smooth (differentiable) after smooth (differentiable) perturbations. With all these concepts, let us consider a Riemannian manifold $V_4$ with a non-perturbed metric $\bar{g}_{\mu\nu}$ being locally and isometrically embedded in a D-dimensional Riemannian manifold $V_n$. The embedded space-time $V_4$ is endowed with the local coordinates $x^\mu = \{x^0, ..., x^3\}$ whereas the extra-dimensions in the bulk space can be defined with the coordinates $x^a = \{x^4, ..., x^{D-1}\}$ and $D = 4+n$. Hence, the bulk local coordinates can be denoted by the set $\{x^\mu, x^a\}$. All these definitions allow us to construct a differentiable and regular map $\mathcal{X} : V_4 \to V_n$ satisfying the embedding equations

$$\mathcal{X}^A_{,\mu}\mathcal{X}^B_{,\nu}\mathcal{G}_{AB} = \bar{g}_{\mu\nu} \ \ , \tag{4}$$

$$\mathcal{X}^A_{,\mu}\bar{\eta}^B_a\mathcal{G}_{AB} = 0 \ \ , \tag{5}$$

$$\bar{\eta}^A_a\bar{\eta}^B_b\mathcal{G}_{AB} = \bar{g}_{ab} \ \ , \tag{6}$$

where the set of $\mathcal{X}^A(x^\mu, x^a) : \mathcal{X}^A = \{\mathcal{X}^0...\mathcal{X}^{D-1}\}$ denotes the non-perturbed embedding function coordinates, the metric $\mathcal{G}_{AB}$ denotes the metric components of $V_D$ in arbitrary coordinates and $\bar{\eta}^A_a$ denotes a non-perturbed unit vector field orthogonal to $V_4$. Concerning notation, capital Latin indices run from 1 to $n$. Small case Latin indices refer to the extra dimension considered. All Greek indices refer to the embedded space-time counting from 1 to 4. Those sets of equations represent, respectively, the isometry condition in Eq.(4), the orthogonality between the embedding coordinates $\mathcal{X}$ and $\bar{\eta}$ in Eq.(5), and also, the vector normalization $\bar{\eta}^A_a$ and $\bar{g}_{ab} = \epsilon_a \delta_{ab}$ with $\epsilon_a = \pm 1$ in which the signs represent the signatures of the extra-dimensions. Hence, the integration of the system of equations Eqs.(4), (5) and (6) assures the configuration of the embedding map $\mathcal{X}$.

The second fundamental form, or more commonly, the non-perturbed extrinsic curvature $\bar{k}_{\mu\nu}$ of $V_4$ is by definition the projection of the variation of $\bar{\eta}$ onto the tangent plane :

$$\bar{k}_{\mu\nu} = -X^A_{,\mu}\bar{\eta}^B_{,\nu}\mathcal{G}_{AB} = X^A_{,\mu\nu}\bar{\eta}^B\mathcal{G}_{AB} \; , \tag{7}$$

where the comma denotes the ordinary derivative.

If one defines a geometric object $\bar{\omega}$ in $V_4$, its Lie transport along the flow for a small distance $\delta y$ is given by $\Omega = \bar{\Omega} + \delta y \pounds_{\bar{\eta}}\bar{\Omega}$, where $\pounds_{\bar{\eta}}$ denotes the Lie derivative with respect to $\bar{\eta}$. In particular, the Lie transport of the Gaussian veilbein $\{X^A_\mu, \bar{\eta}^A_a\}$, defined on $V_4$ gives straightforwardly the perturbed coordinate $\mathcal{Z}^A(x^\mu, y^a) := \mathcal{Z}^A$ such as

$$\mathcal{Z}^A_{,\mu} = X^A_{,\mu} + \delta y^a \; \pounds_{\bar{\eta}} X^A_{,\mu} = X^A_{,\mu} + \delta y^a \; \bar{\eta}^A_{a,\mu} \tag{8}$$

$$\eta^A_a \;\; = \bar{\eta}^A_a + \delta y^b \; [\bar{\eta}_a, \bar{\eta}_b]^A \qquad = \quad \bar{\eta}^A_a \; . \tag{9}$$

It is worth mentioning that Eq.(9) shows that the normal vector $\eta^A$ does not change under orthogonal perturbations. However, from Eq.(7), we note that in general $\eta_{,\mu} \neq \bar{\eta}_{,\mu}$. Likewise, it occurs that the so-called third geometrical form, or more commonly, the torsion vector, $A_{\mu ab}$ does not change under orthogonal perturbations. To see how it works, we take Eq.(13) and rewrite Eq.(5) as

$$g_{\mu b} = \; \mathcal{Z}^A_{,\mu}\eta^B_b\mathcal{G}_{AB} = \; \delta y^a A_{\mu ab} \; , \tag{10}$$

where $\mathcal{Z}^A$ are a set of perturbed coordinates. The Eq.(10) results from a generalization of the Gauss-Weingarten equations

$$\eta^A_{a,\mu} = \; A_{\mu ac}g^{cb}\eta^A_b - \bar{k}_{\mu\rho a}\bar{g}^{\rho\nu}\mathcal{Z}^A_{,\nu} \;\; . \tag{11}$$

then,

$$A_{\mu ab} = \; \eta^A_{a,\mu}\eta^B_b\mathcal{G}_{AB} = \; \bar{\eta}^A_{a,\mu}\bar{\eta}^B_b\mathcal{G}_{AB} = \; \bar{A}_{\mu ab} \;\; , \tag{12}$$

that ratifies that the torsion vector does not alter under perturbations. In geometric language, the presence of a torsion potential tilts the embedded family of submanifolds with respect to the normal vector $\eta^A_a$. If the bulk has certain killing vectors then $A_{\mu ab}$ transforms as the component of a gauge field under the group of isometries of the bulk [24, 61, 62]. It is worth noting that the gauge potential can only be present if the dimension of the bulk space is equal or greater than six ($n \geq 2$) in accordance with Eq.(12) since the torsion vector fields are antisymmetric under the exchange of extra coordinate $a$ and $b$.

To describe the perturbed embedded geometry, we set a perturbed coordinates $\mathcal{Z}^A$ needed to satisfy the embedding equations similar to Eqs.(4), (5) and (6) as

$$\mathcal{Z}^A_{,\mu} Z^B_{,\nu} \mathcal{G}_{AB} = g_{\mu\nu}, \ \mathcal{Z}^A_{,\mu} \eta^B_b \mathcal{G}_{AB} = g_{\mu b}, \ \eta^A_a \eta^B_b \mathcal{G}_{AB} = g_{ab} \ . \tag{13}$$

where $g_{ab} = \epsilon_a \delta_{ab}$ with $\epsilon_a = \pm 1$. Thus, with the Eqs.(13) and using the definition from Eq.(7), one obtains the perturbed metric and extrinsic curvature of the new manifold as written as

$$g_{\mu\nu} = \bar{g}_{\mu\nu} - 2y^a \bar{k}_{\mu\nu a} + \delta y^a \delta y^b \left[\bar{g}^{\sigma\rho} \bar{k}_{\mu\sigma a} \bar{k}_{\nu\rho b} + g^{cd} A_{\mu ca} A_{\nu db}\right] , \tag{14}$$

and the related perturbed extrinsic curvature

$$k_{\mu\nu a} = \bar{k}_{\mu\nu a} - \delta y^b \left(g^{cd} A_{\mu ca} A_{\nu db} + \bar{g}^{\sigma\rho} \bar{k}_{\mu\sigma a} \bar{k}_{\nu\rho b}\right) \ . \tag{15}$$

Taking the derivative of Eq.(14) with respect to $y$ coordinate, one obtains Nash's deformation condition

$$k_{\mu\nu a} = -\frac{1}{2} \frac{\partial g_{\mu\nu}}{\partial y^a} \ . \tag{16}$$

The meaning of this expression is twofold. It can be realized in a pictorial view under the basic theory of curves, i.e., one gets a congruence of curves (or orbits) orthogonal to the embedded space $V_4$. Moreover, the parameter $y$ is time-like or not, and it is irrelevant the sign of its signature. A similar expression was obtained years later in the ADM formulation by Choquet-Bruhat and York [63]. In fact, the physical interpretation of Eq.(16) means that it localizes the matter in the embedded space-time imposing on it a geometric confinement. In other words, it holds true for any perturbations resulting from $n$-parameter families of embedded submanifolds denoted by $y^a$, and the matter remains confined to the resulting perturbed metric that can bend and/or stretch without ripping the manifold (embedded space-time), which can be a valuable feature for a quantization process.

In addition, the integrability conditions for equations in Eq.(13) are given by the non-trivial components of the Riemann tensor of the embedding space expressed in the Gaussian frame $\{\mathcal{Z}^A_{\mu}, \eta^A_a\}$ known as the Gauss-Codazzi-Ricci equations. This guarantees to reconstruct the embedded geometry and understand its properties from the dynamics of the four-dimensional embedded space-time. Consequently, we can define a Gaussian coordinate system $\{\mathcal{Z}^A_{,\mu}, \eta^A_a\}$ for the bulk in the vicinity of $V_4$ in such a way

$$\mathcal{G}_{AB} = \begin{pmatrix} g_{\mu\nu} + g^{ab} A_{\mu a} A_{\nu b} & A_{\mu a} \\ A_{\nu b} & g_{ab} \end{pmatrix} \tag{17}$$

where the perturbed metric $g_{\mu\nu}$ is given by Eq.(14).

The expression in Eq.(17) is the metric of the bulk with $D \geq 6$ or at least two extra-dimensions. This resembles the non-Abelian Kaluza-Klein metric and the quantity $A_{\mu a}$ plays the role of the Yang-Mills potentials where $A_{\mu a} = x^b A_{\mu ab}$. We emphasize that for just one extra-dimension, the torsion vector does not exist and for two extra-dimensions it turns to the usual Maxwell field, which means that the non-Abelian part of $A_{\mu a}$ is lost in a six dimensional bulk. This means that the resulting force is the ordinary electromagnetic one in the case of two extra dimensions [27, 28, 62, 64].

As proposed in [24, 25, 26, 65], one obtains the induced field covariant equations of motion taking Eq.(3) in the frame defined in Eq.(17). In the background for a 4-D observer in the embedded space, we have the following set of equations denoted by Eqs.(18), (19) and (20):

$$G_{\mu\nu} + Q_{\mu\nu} = 8\pi G_N T_{\mu\nu} \ , \tag{18}$$

where the quantity $T_{\mu\nu}$ denotes the stress energy tensors for ordinary intrinsic matter (including Yang-Mills fields).

The second equation involves relations with extrinsic terms $\bar{k}_{\alpha\beta a}$ and $A_{\mu ab}$

$$\nabla^*_\nu \bar{k}_a - \nabla^*_\mu \bar{k}^\mu_{a\nu} = 8\pi G_N T_{a\nu} \ , \tag{19}$$

where the term $\nabla^*_\mu \bar{k}_{\alpha\beta a}$ denotes $\nabla^*_\mu \bar{k}_{\alpha\beta a} := \bar{k}_{\alpha\beta a;\mu} - A_{\mu ab}\bar{k}^b_{\alpha\beta}$ and the semicolon denotes the covariant derivative. Moreover, the third equation is denoted as

$$R + \bar{k}_{\mu\nu m}\bar{k}^{\mu\nu m} - \bar{k}_a\bar{k}^a = -16\pi G_N \eta_{ab} T_{ab} \ , \tag{20}$$

where $\eta_{ab} = \epsilon_a \delta_{ab}$ with $\epsilon_a = \pm 1$. The quantities $G_N$, $T_{a\nu}$, $T_{ab}$ denote the induced gravitational Newton's constant, the stress energy tensors projections of $T_{AB}$ on the cross and normal directions of the space-time, respectively.

Those set of equations are the results from the integrability conditions of the embedding given by the Gauss-Codazzi-Ricci equations. From Nash-Green theorem, the solutions of these equations were obtained by a differentiable process [24]. The first two equations are known, respectively, by the gravi-tensor equation (a modified Einstein's equations by the appearance of the extrinsic curvature) as in Eq.(18) and gravi-vector equation as in Eq.(19). In summary, they reflect the meaning of a dynamical embedding: the pseudo-Riemann curvature of the embedding space acts as a reference for the pseudo-Riemann curvature of the embedded space-time. Moreover, the projection of the Riemann tensor of the embedding space along the normal direction is given by the tangent variation of the extrinsic curvature as shown by Eq.(19) that is the trace of Codazzi equation composed by the extrinsic terms $\bar{k}_{\alpha\beta a}, A_{\mu ab}$. The last equation is known as gravi-Scalar equation and serves as a constrain on the torsion vector fields $A_{\mu ab}$.

The quantity $Q_{\mu\nu}$ is denoted by

$$Q_{\mu\nu} = \bar{g}^{cd}\left(\bar{g}^{\rho\sigma}\bar{k}_{\mu\rho c}\bar{k}_{\nu\sigma d} - \bar{k}_{\mu\nu d}\bar{g}^{\alpha\beta}\bar{k}_{\alpha\beta c}\right) - \frac{1}{2}\left(\bar{k}_{\lambda\phi c}\bar{k}^{\lambda\phi}_{\ \ d} - \bar{g}^{\alpha\beta}\bar{k}_{\alpha\beta d}\bar{g}^{\gamma\delta}\bar{k}_{\gamma\delta c}\right)\bar{g}_{\mu\nu} \ , \tag{21}$$

and is independently conserved quantity in the sense that $Q_{\mu\nu\ ;\nu} = 0$ which means that this geometric new term does not exchange gravitational energy with ordinary matter resembling the quintessence in the dark energy problem. The conservation of $Q_{\mu\nu}$ holds true for perturbed quantities of $g_{\mu\nu}$ and $k_{\mu\nu a}$.

### *2.2. The background cosmological model*

To the present cosmological application, we consider a four-dimensional metric embedded in a five-dimensional bulk to make a proper comparison with the most of cosmological models in literature. In this framework, the set of equations are simplified. The torsion vector $A_{\mu ab}$ does not exist in five-dimensions and Eq.(19) turns to a homogeneous equation and Eq.(20) provides only a relation of consistence between Ricci scalar and extrinsic scalar quantities (no a priori information is gained).

To obtain the embedded four-dimensional equations, one can take Eq.(18) written in the Gaussian frame embedding veilbein $\{\mathcal{X}^A_\mu, \eta^A_a\}$. This reference frame is composed by a regular and differentiable coordinate $\{\mathcal{X}^A_\mu\}$ and a unitary normal vector $\{\eta^A_a\}$. Accordingly, one can obtain the set of the embedded four-dimensional field equations

$$R_{\mu\nu} - \frac{1}{2}Rg_{\mu\nu} - Q_{\mu\nu} = -8\pi G T_{\mu\nu} \ , \tag{22}$$

$$k_{\mu;\rho}^{\ \rho} - h_{,\mu} = 0 \ , \tag{23}$$

where the semi-colon denotes a covariant derivative. The $T_{\mu\nu}$ tensor is the four-dimensional energy-momentum tensor of a perfect fluid, expressed in co-moving coordinates as

$$T_{\mu\nu} = (p+\rho)U_\mu U_\nu + p\, g_{\mu\nu}, \quad U_\mu = \delta^4_\mu \ ,$$

where $U_\mu$ is the co-moving four-velocity. Moreover, the deformation tensor $Q_{\mu\nu}$ is simplified and can given by

$$Q_{\mu\nu} = g^{\rho\sigma}k_{\mu\rho}k_{\nu\sigma} - k_{\mu\nu}H - \frac{1}{2}\left(K^2 - h^2\right) g_{\mu\nu} \ , \tag{24}$$

where we denote $h = g^{\mu\nu}k_{\mu\nu}$ and $h^2 = h.h$ is the mean curvature. The term $K^2 = k^{\mu\nu}k_{\mu\nu}$ is the Gaussian curvature. It follows that $Q_{\mu\nu}$ is conserved in the sense of Noether's theorem

$$Q^{\mu\nu}{}_{;\nu} = 0 \ . \tag{25}$$

Moreover, we work with a spatially Friedman-Lemaître-Robertson-Walker (FLRW) geometry with line element expressed in coordinates $(r, \theta, \phi, t)$ in such a way

$$ds^2 = \ -dt^2 + a^2\left[dr^2 + f^2_\kappa(r)\left(d\theta^2 + \sin^2\theta d\varphi^2\right)\right] \ , \tag{26}$$

where $f(r)_\kappa = \sin r$, r,$\sinh r$. Since the FLRW geometry can be locally embedded in five-dimensions, it can be regarded as a four-dimensional hypersurface dynamically evolving in a flat five-dimensional bulk whose Riemann tensor $\mathcal{R}_{ABCD}$ is

$$\mathcal{R}_{ABCD} = 0 \ , \tag{27}$$

where $\mathcal{G}_{AB}$ denotes the bulk metric components in arbitrary coordinates. Hence, with a flat dimensional bulk, concerning our cosmological applications, we are not considering the appearance of the cosmological constant $\Lambda$.

Using Eq.(26), one obtains a solution for Eq.(23) that is given by

$$k_{ij} = \frac{b}{a^2}g_{ij}, \quad i,j = 1,2,3, \qquad k_{44} = \frac{-1}{\dot{a}}\frac{d}{dt}\frac{b}{a},$$

where the extrinsic bending function $b(t) = k_{11}$ is function of time. The dot symbol denotes an ordinary time derivative. This arbitrariness follows from the confinement of the four-dimensional gauge fields, which produces the homogeneous equation as shown in Eq.(23).

Denoting the usual Hubble parameter by $H = \dot{a}/a$ and the extrinsic parameter $B = \dot{b}/b$, one obtains

$$k_{ij} = \frac{b}{a^2} g_{ij}, \quad k_{44} = -\frac{b}{a^2}(\frac{B}{H} - 1), \tag{28}$$

$$K^2 = \frac{b^2}{a^4}\left(\frac{B^2}{H^2} - 2\frac{B}{H} + 4\right), \quad h = \frac{b}{a^2}(\frac{B}{H} + 2) \tag{29}$$

$$Q_{ij} = \frac{b^2}{a^4}\left(2\frac{B}{H} - 1\right) g_{ij}, \; Q_{44} = -\frac{3b^2}{a^4}, \tag{30}$$

$$Q = -(K^2 - h^2) = \frac{6b^2}{a^4}\frac{B}{H}\,, \tag{31}$$

where in Eq.(30), we have denoted $i, j = 1..3$, with no sum in indices. For simplicity, we denote the expansion parameter as $a(t) = a$ and the bending function as $b(t) = b$.

Since the dynamics equations for the extrinsic curvature are not complete in five-dimensions, motivated by the lack of uniqueness of the function $b(t)$, and being the extrinsic curvature independent rank-2 field, one can derive the Einstein-Gupta equations [29, 66] in a form

$$\mathcal{F}_{\mu\nu} = 0\,, \tag{32}$$

where they are defined as a copy (concerning its structure) of the usual Riemannian geometry. Hence, once can define a "f-Riemann tensor"

$$\begin{aligned} \mathcal{F}_{\nu\alpha\lambda\mu} &= \partial_\alpha \Upsilon_{\mu\lambda\nu} - \partial_\lambda \Upsilon_{\mu\alpha\nu} + \Upsilon_{\alpha\sigma\mu}\Upsilon^\sigma_{\lambda\nu} - \Upsilon_{\lambda\sigma\mu}\Upsilon^\sigma_{\alpha\nu}\,, \\ \Upsilon_{\mu\nu\sigma} &= \frac{1}{2}\left(\partial_\mu f_{\sigma\nu} + \partial_\nu f_{\sigma\mu} - \partial_\sigma f_{\mu\nu}\right) \qquad\qquad , \\ \Upsilon_{\mu\nu}{}^\lambda &= f^{\lambda\sigma}\,\Upsilon_{\mu\nu\sigma}. \end{aligned}$$

that were constructed from a "connection" associated with $k_{\mu\nu}$ and

$$f_{\mu\nu} = \frac{2}{K} k_{\mu\nu}, \quad \text{and} \quad f^{\mu\nu} = \frac{2}{K} k^{\mu\nu}\,, \tag{33}$$

in such a way that the normalization condition $f^{\mu\rho} f_{\rho\nu} = \delta^\mu_\nu$ applies.

### *2.3. The modified Friedmann equation*

Taking Eq.(26) in Eq.(32), ones obtains the contribution $\frac{B}{H} = 1 \pm \sqrt{|4\eta_0 a^4 - 3}$, and with the results from Eqs.(22), (23) and (25), the Friedmann equation modified by the extrinsic curvature can be written as

$$\left(\frac{\dot{a}}{a}\right)^2 = \frac{8}{3}\pi G\rho + \alpha_0 a^{2\beta_0 - 4} e^{\gamma^{\pm}(t)}\,, \tag{34}$$

where $\alpha_0$ denotes an integration constant and its value is set to 1 without loss of generality. Concerning the total energy $\rho$, we denote $\rho = \rho_{mat} + \rho_{rad}$, which are the matter and radiation energy densities. The $\gamma$-exponent in the exponential function in Eq.(34) is defined as $\gamma^{\pm}(t) = \pm\sqrt{|4\eta_0 a^4 - 3|} \mp \sqrt{3}\arctan\left(\frac{\sqrt{3}}{3}\sqrt{|4\eta_0 a^4 - 3|}\right)$ and the relation of expansion scale factor with redshift is given by $a = \frac{1}{1+z}$. The parameter $\beta_0$ inflicts on the magnitude of the deceleration parameter $q(z)$ in function of the redshift $z$ and the parameter $\eta_0$ measures the width of the transition phase redshift $z_t$ from a decelerating to accelerating regime. Moreover, we can write Friedman equations as

$$H(z) = H_0\sqrt{\Omega_m(z) + \Omega_{rad}(z) + \Omega_{ext}(z)e^{\pm\gamma(z)}}\ , \tag{35}$$

where $H(z)$ is the Hubble parameter in terms of redshift $z$ and $H_0$ is the current value of the Hubble constant. The matter density parameter is denoted by $\Omega_m(z) = \Omega_m^0(1+z)^3$, $\Omega_{rad}(z) = \Omega_{rad}^0(1+z)^4$ with $\Omega_{rad}^0 = \Omega_m^0 z_{eq}$ and the term $\Omega_{ext}(z) = \Omega_{ext}^0(1+z)^{4-2\beta_0}\gamma_0$ stands for the density parameter associated with the extrinsic curvature. The upper script "0" indicates the present value of any quantity. The equivalence number for the expansion factor $a_{eq}$ given by

$$a_{eq} = \frac{1}{1+z_{eq}} = \frac{1}{(1 + 2.5\times 10^4\Omega_m h^2(T_{cmb}/2.7)^{-4})} \tag{36}$$

where $z_{eq}$ is the equivalence redshift. The CMB temperature we adopt the value $T_{cmb} = 2.7255K$ and $h = 0.67$. The complete form for Hubble parameter as in Eq.(35) has been investigated in a sequence of studies [29, 31, 32, 34, 67].

The transition redshift can be found from the deceleration parameter in a form

$$q(z) = \frac{1}{H(z)}\frac{dH(z)}{dz}(1+z) - 1\ . \tag{37}$$

Hence, we can write

$$q(z) = \frac{3}{2}\left[\frac{\Omega_{\ m}(z) + \Omega_{rad}(z) + \gamma^*\Omega_{\ ext}(z)}{\Omega_{\ m}(z) + \Omega_{rad}(z) + \Omega_{\ ext}(z)}\right] - 1\ \ , \tag{38}$$

where $\gamma^* = \frac{1}{3}\left[4 - 2\beta_0 \pm 2\sqrt{|\frac{4\eta_0}{(1+z)^4} - 3|}\ \right]$.

Analyzing the form of the $\gamma^{\pm}(z)$, an estimative for the magnitude of the width of the transition redshift $z_d$ can given by the constraint

$$z_d = |\left(\frac{4}{3}|\eta_0|\right)^{(1/4)} - 1| \leq 1\ . \tag{39}$$

In this work, we investigate an initial late-time transition redshift $z_t \sim 1$ since the constraint of Eq.(39) imposes a small value the parameter $\eta_0 \sim 0$. Thus, the Hubble function in Eq.(35) can be analytically expanded in a Mclaurin-Puiseux series with $\eta_0 \to 0$ truncating at second order, i.e, $e^{\gamma(x(a))} \sim 1 + \frac{\sqrt{3}}{3}x(a)^{3/2} + \mathcal{O}(x^{5/2})$. Considering only the linear terms, it gives roughly $e^{\gamma(z)} \sim \gamma_0(z+1)^{-4}$, which $\gamma_0$ is a constant (with the $\eta_0$ parameter included). The convergence of $e^{\gamma(a)}$ is in compliance with the Walsh theorem on convergence of analytic approximations [68].

The current extrinsic contribution $\Omega_{ext}^0$ is given by the normalization condition for redshift at $z = 0$ that results in

$$\Omega_{ext}^0 = \frac{2}{\eta_0}\left(1 - \Omega_m^0 - \Omega_{rad}^0\right)\ . \tag{40}$$

Hence, we can write the dimensionless Hubble parameter $E(z) = \frac{H(z)}{H_0}$ as

$$E^2(z) = \Omega_m^0(1+z)^3 + \Omega_{rad}^0(1+z)^4 + \left(1 - \Omega_m^0 - \Omega_{rad}^0\right)(1+z)^{-2\beta_0} . \quad (41)$$

## 3. Observational constraints: analysis and results

### 3.1. Cosmological data

The methodology used to handle the data relies on the Markov Chain Monte Carlo (MCMC) technique based on the Metropolis-Hasting algorithm. We perform our analysis using the joint likelihood of the CMB Planck 2015 data [1], Pantheon SnIa [41], the Hubble parameter as a function of redshift $(H(z))$[42, 43, 44, 45, 46, 47] and Baryonic Acoustic Oscillations (BAO) from points of the joint surveys 6dFGS [48], SDDS [49], BOSS CMASS [50], WiggleZ [51], MSG [52] and BOSS DR12 [53].

To apply our $\chi^2$-statistics, we have a total of 1096 data points from the Pantheon set, CMB, BAO and Hubble parameter with the number of point of 1048, 3, 9 and 36, respectively. Hence, we use the background parameter vectors $\{\Omega_{m0}, 100\Omega_b h^2, \beta_0, \eta_1\}$, which the adopted priors were $\{(0.001, 1), (0.001, 0.08), (-0.3, 1), (0.01, 0.5)\}$, respectively. For convenience of notation, we denote the "normalized" parameter $\eta_1 = 100\eta_0$ heron. Moreover, to implement the MCMC chains, the joint analysis is defined by the product of the particular likelihoods $\mathcal{L}$ for each data set

$$\mathcal{L}_{tot} = \mathcal{L}_{Pantheon}.\mathcal{L}_{BAO}.\mathcal{L}_{CMB}.\mathcal{L}_{H(z)} , \quad (42)$$

and the sum of individual $\chi^2$ to get the related total $\chi^2$

$$\chi^2_{tot} = \chi^2_{Pantheon} + \chi^2_{BAO} + \chi^2_{CMB} + \chi^2_{H(z)}. \quad (43)$$

The adopted values for the $H(z)$ data can be found in Table 1 of the ref.[40].

The related absolute magnitude $M$ is given by

$$m(z) = M + 5\ log_{10}[\frac{d_L(z)}{Mpc}] + 25 \quad (44)$$

The luminosity distance $D_L$ is defined by

$$D_L(z) = \frac{H_0 d_L(z)}{c} \quad (45)$$

as

$$m(z) = \bar{M}(M, H_0) + 5\ log_{10}(D_L(z)) \quad (46)$$

where $\bar{M}$ is the magnitude zero point offset and depends on $M$ and $H_0$ as

$$\bar{M} = M + 5\ log_{10}(\frac{c/H_0}{1Mpc}) + 25 \quad (47)$$

The $\bar{M}$ is model independent and its value comes from a specific good fit that can be used directly to other fits of model parameters. Hence, the observed $m_i(z_i)$ can be translated to $D_{Li}^{obs}(z_i)$ and its value $D_L^{th}(z)$ of a given model $H(z; \alpha_1, ..., \alpha_n)$ can be obtained by integrating

$$D_L^{th}(z) = (1+z)\int_0^z dz' \frac{H_0}{H(z'; \alpha_1, ...\alpha_n)} \quad (48)$$

**Table 1.** A compilation of the Hubble function $H(z)$ data used in the current analysis (in units of km.$s^1$ $Mpc^1$). The relatives error points are denoted by the $\sigma_H$ column. The references of the data points can be found in Table 1 of the ref.[40].

| redshift | $H(z)$ | $\sigma_H$ | redshift | $H(z)$ | $\sigma_H$ |
|---|---|---|---|---|---|
| 0.07 | 69 | 19.6 | 0.57 | 96.8 | 3.4 |
| 0.09 | 69.0 | 12.0 | 0.593 | 104.0 | 13.0 |
| 0.12 | 68.6 | 26.2 | 0.60 | 87.9 | 6.1 |
| 0.12 | 68.6 | 26.2 | 0.68 | 92.0 | 8.0 |
| 0.179 | 75.0 | 4.0 | 0.73 | 97.3 | 7.0 |
| 0.199 | 75.0 | 5.0 | 0.781 | 105.0 | 12.0 |
| 0.2 | 72.9 | 29.6 | 0.875 | 125.0 | 17.0 |
| 0.27 | 77.0 | 14.0 | 0.88 | 90.0 | 40.0 |
| 0.28 | 88.8 | 36.6 | 0.9 | 117.0 | 23.0 |
| 0.35 | 82.7 | 8.4 | 1.037 | 154.0 | 20.0 |
| 0.352 | 83.0 | 14.0 | 1.3 | 168.0 | 17.0 |
| 0.3802 | 83.0 | 13.5 | 1.363 | 160.0 | 33.6 |
| 0.4 | 95.0 | 17.0 | 1.43 | 177.0 | 18.0 |
| 0.4004 | 77.0 | 10.2 | 1.53 | 140.0 | 14.0 |
| 0.4247 | 87.1 | 11.2 | 1.75 | 202.0 | 40.0 |
| 0.44 | 82.6 | 7.8 | 1.965 | 186.5 | 50.4 |
| 0.44497 | 92.8 | 12.9 | 2.34 | 222.0 | 7.0 |
| 0.4783 | 80.9 | 9.0 | | | |
| 0.48 9 | 7.0 | 62.0 | | | |

The best fit values for the parameters $\alpha_1, ..., \alpha_n$ are found by minimizing the quantity

$$\chi^2(a_1, ..., a_n) = \sum_{i=1}^{N} \frac{(log_{10}D_L^{obs}(z_i) - log_{10}D_L^{th}(z_i))^2}{(\sigma_{log_{10}D_L(z_i)})^2 + (\frac{\partial log_{10}D_L(z_i)}{\partial z_i}\sigma_{z_i})^2} \tag{49}$$

where $\sigma_z$ is the $1\sigma$ redshift uncertainty of the data and $\sigma_{log_{10}D_L(z_i)}$ is the corresponding $1\sigma$ error of $log_{10}D_L^{obs}(z_i)$.

### *3.2. Results and discussions*

In order to avoid an error-prone fit-to-data, we must correlate the parameters $\beta_0$ and $\eta_0$. To this matter, we define a parameterization in a form

$$\beta(a) = -1 - \frac{2}{3}\beta_0 + \eta_0(1-a)\ . \tag{50}$$

To facilitate the analysis, the $\beta_0$ parameter, that is a parameter originated from a geometric part, is related to the fluid parameter $w$ with the formula $\beta_0 = \frac{3}{2}(1+w)$. Accordingly, the values of $\beta_0$ runs from -0.3 to 1 means roughly $-1/3 \leq w \leq -1.2$ in fluid context and varies from a quintessence to a phantom fluid. The $\Lambda$CDM model corresponds to $w = -1$ or, equivalently, $\beta_0 = 0$ in Eq.(50). We compare our results with three phenomenological models to ascertain on how the $\beta$-model is constrained to the available data. In table 1, we present the values of parameters of the $\Lambda$CDM model, and $w$CDM and CPL parameterisations. In figures 1 and 2, the comparisons are made with the models from left-to-right sequence in the panels.

In figure 1, we present the obtained $\sigma$-contours with $68,3\%$, $95,4\%$ and $99,7\%$ confidence levels (C.L.) in the $(\beta_0 - \Omega_m)$ plane. We refer to the present model as the $\beta_0$ model, for short, as intended to be in comparison with some popular models in literature. In the first and second panels, we have the comparison with $\Lambda$CDM and $w$CDM models and the marginalized $\beta_0$ is within the 1-$\sigma$ contour (black point). The red points represent the models in comparison. The comparison with $\Lambda$CDM, the $\sigma$-distance between the models reaches the limiting 1-$\sigma$ border. In the case of $w$CDM, the red point extrapolates and reaches the 3-$\sigma$ contour leading to a statistical tension between the models. A different pattern occurs in the figure 2, which may represent a mild tension between low redshift data ($H(z)$) and the Planck probe [40, 69]. In terms of a comparison with the accommodation of the baryonic luminous matter parameter $\Omega_b h^2$ with the distribution of the matter density parameter $\Omega_m$, we have a well-behaved predictions at 1-$\sigma$ level for all models in the plane $(\Omega_b h^2 - \Omega_m)$.

In order to classify the correlation between models, we adopt the errors being as Gaussian. Thus, we use AIC systematic to classify the fit-to-data for small samples sizes [70, 71]

$$AIC = \chi^2_{bf} + 2k\frac{2k(k+1)}{N-k-1} , \tag{51}$$

where $\chi^2_{bf}$ is the best fit $\chi^2$ of the model, $k$ represents the number of the free parameters and $N$ is the number of the data point in the adopted dataset. The difference $|\Delta AIC| = AIC_{model\ 2} - AIC_{model\ 1}$ obeys the Jeffreys' scale [72] that measures the intensity of tension between two competing models. In general, higher values for $|\Delta AIC|$ denotes more tension between models, that means a higher statistical distance and the models are not statistically compatible.

In summary, the Jeffreys' scale can be set in the following: for $|\Delta AIC \leq 2|$ the models are statistically consistent and equivalents. For $4 < \Delta AIC < 7$ and $|\Delta AIC \geq 10|$ induces to growing tension between the models with positive evidence and strong evidence against the equivalence of the models, respectively. Accordingly, we have obtained the values for the $\beta$-$\Lambda$CDM with 1.93, and $\beta$-$w$CDM and $\beta$-CPL with $\Delta$AIC 1.79 and 0.11, respectively. This result leads to the conclusion that the $\beta$-model favors CPL parameterization with a lower $\Delta$AIC, even though it is shown that the $\beta$-model is statistically consistent (weak tension) with $\Lambda$CDM and $w$CDM models. Likewise, we apply BIC classifiers [55] that work well for independent homogeneous distribution of datasets [71]. Unlike AIC methodology, the BIC method heavily penalizes free parameters of a model. Thus, we use the following formula

$$BIC = \chi^2_{bf} + k\ln N , \tag{52}$$

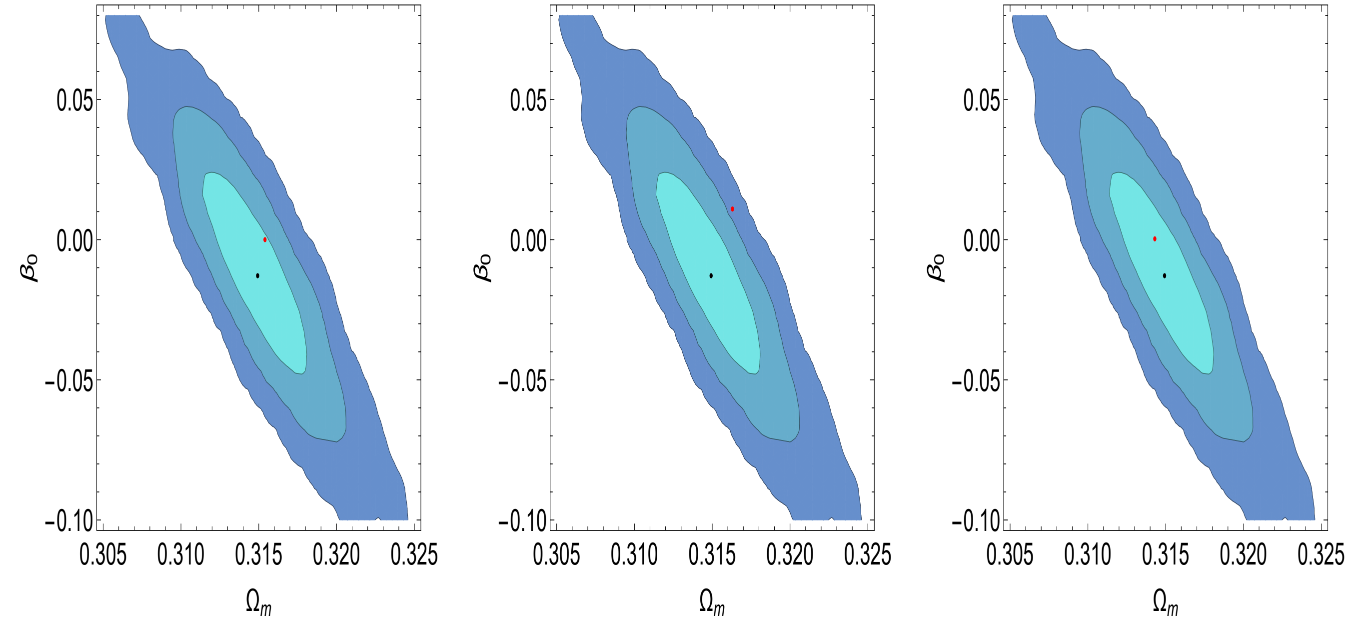


**Figure 1.** Contour regions at 1-$\sigma$, 2-$\sigma$ and 3-$\sigma$ at 68, 3%, 95, 4% and 99, 7% C.L. in the $(\beta_0 - \Omega_m)$ plane. The points represent the mean values of the parameters in the MCMC chain. The black points denote the $\beta$-model and the red points denote the comparison models and from left-to-right, we have $\Lambda$CDM, $w$CDM and CPL models, respectively.

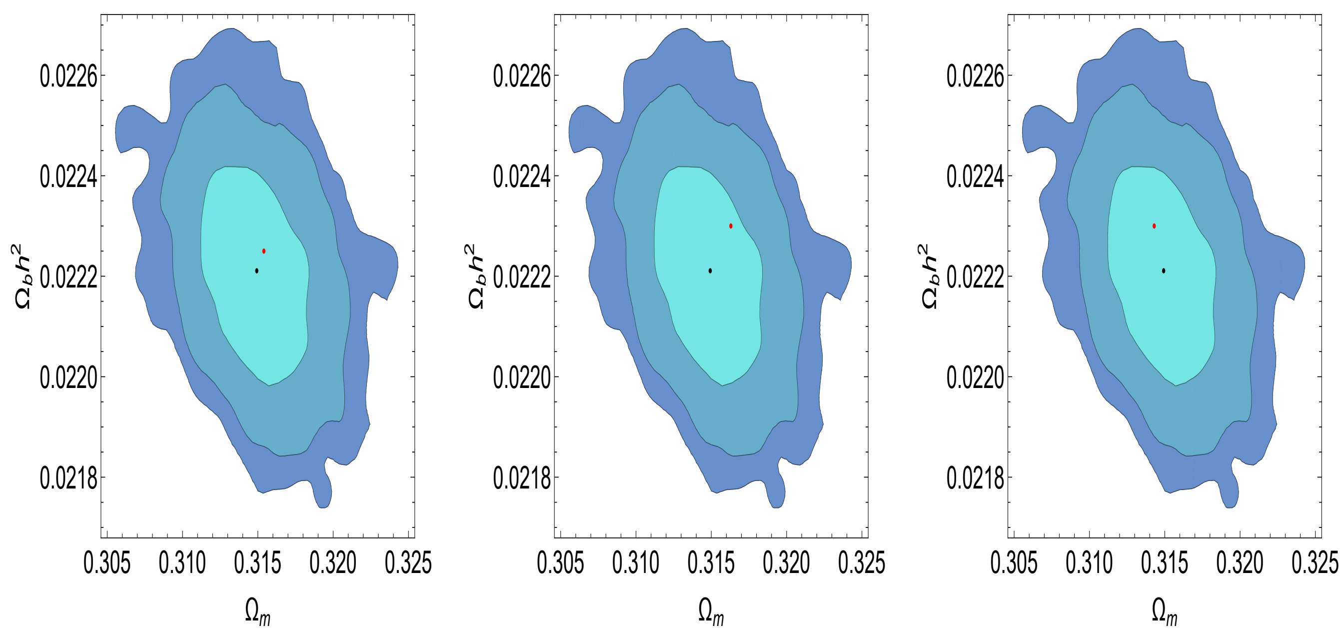


**Figure 2.** Contour regions at 1-$\sigma$, 2-$\sigma$ and 3-$\sigma$ at 68, 3%, 95, 4% and 99, 7% C.L. in the $(\Omega_b h^2 - \Omega_m)$ plane.

**Table 2.** A summary of best-fit values background parameters calculated by using MCMC chains with the main parameters and resulting $\chi^2$ values. The $\chi^2_{min}$ denotes the $\chi^2$ best-fit value from MCMC and $\chi^2_{tot}$ refers to the value of the total $\chi^2$ from minimizing all data. For the sake of convenience, we refer the present model in this paper as $\beta$-model as shown below.

| Model | $\Omega_{m0}$ | $\Omega_{b0}h^2$ | DE parameters | $\chi^2_{min}$ | $\chi^2_{tot}$ |
|---|---|---|---|---|---|
| $\Lambda$CDM | 0.3154± 0.0061 | 0.0222± 0.0001 | $w=-1$ | 1809.67 | 1809.75 |
| $w$CDM | 0.3163± 0.0081 | 0.0223± 0.0015 | $w$=-0.9927± 0.0268 | 1809.81 | 1809.75 |
| CPL | 0.3143± 0.0061 | 0.0223± 0.0001 | $w$=-0.9998± 0.0008<br>$wa$=-0.0166± 0.0080 | 1809.69 | 1809.75 |
| $\beta$-model | 0.3144± 0.0023 | 0.0223± 0.0001 | $\beta_0$=-0.0059± 0.0245<br>$\eta_1$=0.2884± 0.0055 | 1809.58 | 1809.80 |

**Table 3.** A summary of mean values of background parameters calculated by using MCMC chains with the main parameters.

| Model | $\Omega_{m0}$ | $\Omega_{b0}h^2$ | $h$ | DE parameters |
|---|---|---|---|---|
| $\Lambda$CDM | 0.3179± 0.0065 | 0.0223± 0.0001 | 0.6694± 0.0051 | $w=-1$ |
| $w$CDM | 0.3163± 0.0081 | 0.0223± 0.0015 | 0.6717± 0.0074 | $w$=-0.9927± 0.0268 |
| CPL | 0.3134± 0.0062 | 0.0222± 0.0001 | 0.6752± 0.0046 | $w$=-0.9996± 0.0008<br>$wa$=-0.0166± 0.008 |
| $\beta$-model | 0.3149± 0.0097 | 0.0222± 0.0001 | 0.6730± 0.0082 | $\beta_0$=-0.0128± 0.0299<br>$\eta_1$=0.2998± 0.0079 |

**Table 4.** A summary of the obtained values of AIC and BIC for the studied models.

| Model | $AIC$ | $\Delta AIC$ | Tension | $BIC$ | $\Delta BIC$ | Tension |
|---|---|---|---|---|---|---|
| $\Lambda$CDM | 1817.71 | 1.93 | weak | 1837.67 | 6.91 | growing |
| $w$CDM | 1817.85 | 1.79 | weak | 1837.81 | 6.77 | growing |
| CPL | 1819.75 | 0.11 | mild | 1844.69 | 0.11 | mild |
| $\beta$-model | 1819.64 | 0 | - | 1844.58 | 0 | - |

where $\chi^2_{bf}$ is the best fit $\chi^2$ of the model, $k$ represents the number of the free parameters and $N$ is the number of the data point in the adopted dataset. Therefore, from Jeffrey's scale, a smaller ΔBIC values favor statistically better models (lower tension between two comparison models). In these terms, we have similar results as those obtained from AIC, with ΔBIC of the order of 0.11, except for the cases of $\Lambda$CDM and $w$CDM which the comparison in BIC analysis gives the values 6.91 and 6.77 indicating a growing tension between the models. Particulary, the tension is a little higher with the $\Lambda$CDM model, that shows a non-preferable tendency for non-dynamical dark energy models, besides the fact that the BIC analysis has a severe sensitivity on free parameters. The table III shows a summary of AIC and BIC values for the models and the corresponding tension between the models. In the figure 03, we present the marginalized $\eta_1$ in the $(\eta_1 - \Omega_m)$

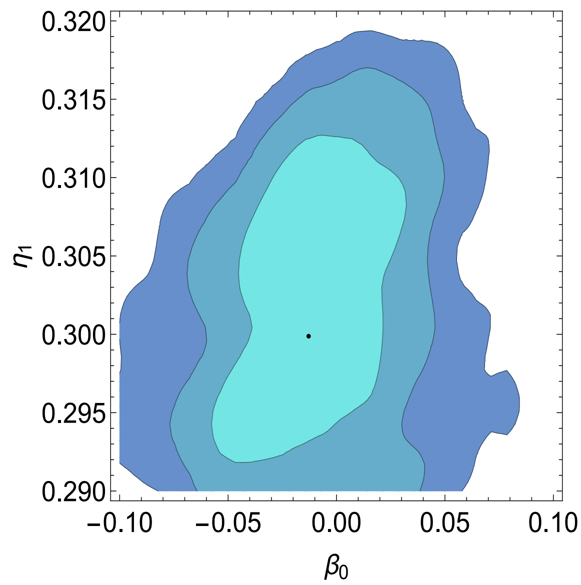


**Figure 3.** Contour regions at 1-$\sigma$, 2-$\sigma$ and 3-$\sigma$ at 68, 3%, 95, 4% and 99, 7% C.L. in the ($\eta_1 - \beta_0$) plane. The point represents the mean values of the parameters in the MCMC chain accommodated in the 1-$\sigma$ contour.

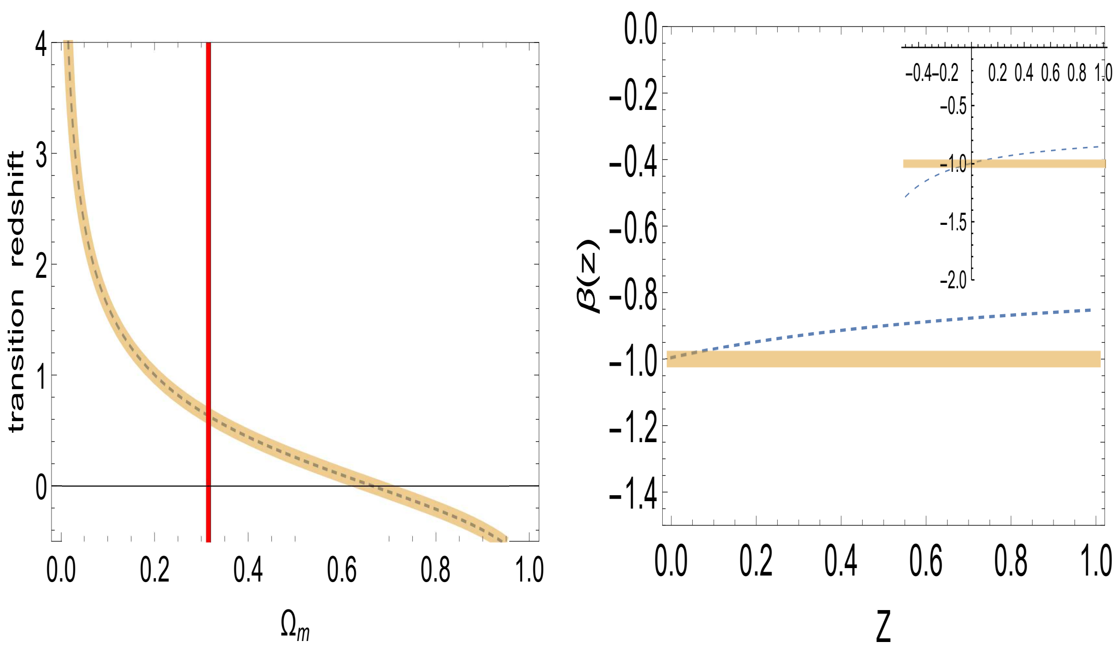


**Figure 4.** Right: Transition redshift as a function of the matter density parameter for a spatially flat Universe with $z_t = 0.634 \pm 0.014$. Left: the behaviour of the $\beta(z)$ function in terms of redshift. In the minor panel, it shows an extrapolation of the $\beta(z)$ function for a remote future $z \sim -1$. In both panels, the dash line represents the $\beta$-model, and the thick line denotes $\Lambda$CDM.

well-accommodated in the 1-$\sigma$ contour.

In the figure 04, it is shown the behaviour of the transition redshift $z_t$ in terms of the matter distribution $\Omega_m$. Taking equation Eq.(38) and calculating the deceleration parameter $q(z)=0$, we can find the transition redshift $z_t$ as

$$z_t = \left[\frac{2(1+\beta_0)(1-\Omega_{m0})}{\Omega_{m0}}\right]^{\frac{1}{2\beta_0+3}} - 1\,. \tag{53}$$

The compatible value in accordance with Planck results[1] with $z_t = 0.634 \pm 0.014$ at 1-$\sigma$ with a narrow window of the matter distribution $\Omega_m = 0.3144 \pm 0.0023$. This is also in accordance with independent fits in literature as in, e.g., with $z_t = 0.64^{+0.11}_{-0.07}$ [73], and BAO/CMB + SNIa constraints, with MLCS2K2 light-curve fitter it gives $z_t = 0.56^{+0.13}_{-0.10}$ and with SALT2 fitter, $z_t = 0.64^{+0.13}_{-0.07}$ with 68% C.L [74]. Moreover, in the left panel in figure 04, we present the behaviour of the $\beta(z)$ function in terms of redshift thats shows a close concordance with $\Lambda$CDM what refers to the proximity to the value $w=-1$ for the present day, as well as the $w$CDM and CPL parameterization, but for future and intermediate redshifts it clearly show a dynamical aspect of the $\beta$ model departing from $\Lambda$CDM.

## 4. Remarks

In this paper, we discussed the dark energy problem with a proposal of a geometric model for the accelerated expansion. By construction, we used the Nash-Green theorem to propose a geometric model with a resulting modified Friedman equation from the influence of the extrinsic curvature thought as a complement to Einstein's gravity. Starting from the possibility to relate one free parameter to the redshift transition $z_t$, we investigated the possibility that the equation of state undergoes to intermediate redshifts $z_t \lesssim 1$ eventually. In all cases, we applied the AIC and BIC classifies and we found that the model favours the CPL parameterization in which is statistically compatible. Interestingly, we obtained that the transition redshift acts like important parameter in the acceleration expansion and may be used as a cosmic descriptor. This transition occurred in $z_t = 0.634 \pm 0.014$ with a marginalized $\eta_1$ for the best-fit. As future prospects, we intend to investigate that the transition redshift range may inflict changes in the ISW contribution as different as the one as predicted to $\Lambda$CDM with a lower peak of the second CMB peak. Also, the evolution of the background with the evaluation of the cosmological perturbations are import to investigate to confront the behaviour of the viscosity parameter and growth index rate resulting from the $\beta$-model to a realistic one. This process is in due course and will be reported elsewhere.

## 5. Acknowledgments

The author thanks Federal University of Latin-American Integration for financial support from Edital PRPPG 110 (17/09/2018) and Fundação Araucária/PR for the Grant CP15/2017-P&D 67/2019.

## 6. References

[1] Ade P. A. R. et al., (Planck Collaboration), 2016, Astron. Astrophys. 594, A13.
[2] Nemiroff R. J., Joshi R., Atla B.R., 2015, JCAP06, 006.
[3] Santos B., Coley A. A., Devi C. N., Alcaniz J.S., 2017, JCAP02, 047.
[4] Kumar P., Singh C. P., 2017, Astrophys Space Sci., 362, 52.
[5] Velten H.E.S., vom Marttens R.F., Zimdahl W., 2014, Eur.Phys.J. C74, 11, 3160.
[6] Sultana J., 2016, Mon.Not.Roy.Astron.Soc. 457(1), 212-216.
[7] Sivanandam N., 2013, Phys. Rev. D 87, 083514.
[8] Nozari K., Behrouz N., Rashidi N., 2014, Adv. High En.Phys., Article ID 569702.
[9] Martins C. J. A. P., Colomer P. M., 2016, A&A, 594, A14.
[10] Martins C. J. A. P., Colomer P. M., 2018, A&A, 616, A32.
[11] Martins C. J. A. P., Colomer P. M., 2019, Phys. Lett. B, 791, 230-235.
[12] Hill C.T., Schramm D. N., Fry J.N., 1988, Comments Nucl. Part. Phys., 19, 25, 407.
[13] Bassett A. B., Kunz M., Silk J., Ungarelli C., 2002, Mon. Not. R. Astron. Soc. 336, 1217-1222.
[14] Parker L., Raval A., 1999, Phys. Rev. D60, 123502, 1999 [Erratum: Phys. Rev.D67,029902 (2003).
[15] Parker L., Raval A., 2000, Phys. Rev. D62, 083503. [Erratum: Phys. Rev.D67,029903(2003)]
[16] Mortonson M. J., Hu W., Huterer D., 2009, Phys. Rev. D80, 067301.
[17] Di Valentino E., Linder E. V., Melchiorri A., 2018, Phys. Rev. D97, 043528.
[18] Durrive J.-B., Ooba J., Ichiki K., Sugiyama N., 2018, Phys. Rev. D97, 043503.
[19] Arkani-Hamed N., Dimopoulos S., Dvali G., 1998, Phys. Lett., B429, 263.
[20] Randall L., Sundrum R., 1999, Phys. Rev. Lett. 83, 3370.
[21] Randall L., Sundrum R., 1999, Phys. Rev. Lett., 83, 4690.
[22] Dvali G., Gabadadze G., Porrati M., 2000, Phys. Lett.B485, 208-214.
[23] Battye R. A., Carter B., 2001, Phys. Lett. B, 509, 331.
[24] Maia M. D., Monte E. M., 2002, Phys. Lett. A, 297, 2, 9-19.
[25] Maia M.D., Monte E.M., Maia J.M.F., Alcaniz J.S., 2005, Class.Quantum Grav., 22, 1623.
[26] Maia M.D., Silva N., Fernandes M.C.B., 2007, JHEP, 04, 047.
[27] Heydari-Fard M., Sepangi H. R., 2007, Phys.Lett.B649, 1-11.
[28] Jalalzadeh S., Mehrnia M., Sepangi H. R., 2009, Class.Quant.Grav., 26,155007.
[29] Maia M. D., Capistrano A. J. S., Alcaniz J. S., Monte E. M., 2011, Gen. Rel. Grav., 10, 2685.
[30] Ranjbar A., Sepangi H. R., Shahidi S., 2012, Ann. Phys., 327, 3170-3181.
[31] Capistrano A. J. S., Cabral L. A., 2014, Ann. Phys., 384, 64-83.
[32] Capistrano A. J. S., 2015, Montl. Not. Roy. Soc, 448, 1232-1239.
[33] Capistrano A. J. S., Gutiérrez-Pieres A. C., Ulhoa S. C., Amorim R. G. G., 2017, Ann. Phys., 380, 106120.
[34] Capistrano A. J. S., 2017, Ann. Phys. (Berlin), 1700232.
[35] Caldwell R. R., Dave R., Steinhardt P. J., 2018, Phys. Rev. Lett. 80, 1582.
[36] Ratra B., Peebles P. J. E., 1988, Phys. Rev. D 37, 3406.
[37] Chevallier M., Polarski D., 2001, Int. J. Mod. Phys. D 10, 213.
[38] Linder E. V., 2003, Phys. Rev. Lett., 90, 091301.
[39] Luna C. A., Basilakos S., Nesseris S., 2018, Phys. Rev. D 98, 023516.
[40] Arjona R., Cardona W., Nesseris S., 2019, Phys. Rev. D 99, 043516.
[41] Scolnic D. M. et al., 2018, Astrophys. J. 859, 101 (2018), 1710.00845.
[42] Zhang C., Zhang H., Yuan S., Zhang T. J., Sun Y.-C., 2014, Res. Astron. Astrophys. 14, 1221, 1207.4541.
[43] Stern D., Jimenez R., Verde L., Kamionkowski M., Stanford S. A., 2010, JCAP 1002, 008.
[44] Moresco M. et al., 2012, JCAP 1208, 006.
[45] Chuang C.H., Wang Y., 2013, Mon. Not. Roy. Astron. Soc. 435, 255.
[46] Moresco M., 2015, Mon. Not. Roy. Astron. Soc. 450, L16.
[47] Delubac T. et al. (BOSS collaboration), 2015, Astron. Astrophys. 574, A59.

[48] Beutler F. et al., 2011, Mon. Not. Roy. Astron. Soc. 416, 3017.
[49] Anderson L. et al., 2014, (BOSS collaboration), Mon. Not. Roy. Astron. Soc.441, 24.
[50] Xu X., Padmanabhan N., Eisenstein D. J., Mehta K. T., Cuesta A. J., 2012, Mon. Not. Roy. Astron. Soc. 427, 2146.
[51] Blake C. et al., 2012, Mon. Not. Roy. Astron. Soc. 425, 405.
[52] Ross A. J. at al., 2015, Mon. Not. Roy. Astron.Soc. 449, 835.
[53] Gil-Marín H. et al., 2016, Mon. Not. Roy. Astron. Soc. 460, 4210.
[54] Akaike H., 1974, IEEE Transactions of Automatic Control, 19, 716.
[55] Schwarz G., 1978, Ann. Statist., 5, 461.
[56] Donaldson S. K., 1984, Contemporary Mathematics (AMS), 35, 201.
[57] Taubes C. H., 1984, Contemporary Mathematics (AMS), 35, 493.
[58] Lim C. S., 2014, Prog. Theor. Exp. Phys., 02A101.
[59] Nash J., 1956, Ann. Maths., 63, 20.
[60] Greene R., 1970, Memoirs Amer. Math. Soc., 97.
[61] Holdom B., 1983, *the cosmological constant and the embedded universe*, Standford preprint ITP-744.
[62] Jalalzadeh S., Vakili B., Sepangi H. R., 2007, Phys. Scr., 76, 122.
[63] Choquet-Bruhat Y., Jr York J., 1997, Mathematics of Gravitation, Warsaw: Institute of Mathematics, Polish Academy of Sciences.
[64] Maia M.D., IJMPA, Vol. 31, 1641010 (2016); D. C. N. Cunha, M. D. Maia, Massive Kaluza-Klein Gravity, [Arxiv: 1310.8525v1]
[65] Jalalzadeh S., Rostami T., 2015, IJMPD, 24, 4, 1550027.
[66] Gupta S. N., 1954, Phys. Rev., 96, 6.
[67] Capistrano A. J. S., Cabral L. A., 2016, Class. Quantum Grav. 33, 245006.
[68] Walsh J.L., 1928, Trans. Amer. Math. Sot. 30, 307-332.
[69] Nesseris S., Pantazis G., Perivolaropoulos L., 2017, Phys. Rev. D 96, 023542.
[70] Sugiura N., 1978, Communications in Statistics A, Theory and Methods, 7, 13.
[71] Liddle A. R., 2007, Mon. Not. R. Astron. Soc. 377, L74L78.
[72] Jeffreys H., 1961, Theory of Probability, 3rd edn. Oxford Univ. Press, Oxford.
[73] Moresco M. at al., 2016, JCAP, 05, 014.
[74] Giostri R. et al., 2012, JCAP, 1203, 027.